Tertiary Chiral Domains Assembled by Achiral Metal−Organic Complexes on Cu(110)

Yeliang Wang,[†,‡] Stefano Fabris,[§] Giovanni Costantini,*[,†,∥] and Klaus Kern[†,⊥]

Max-Planck-Institut für Festkörperforschung, Heisenbergstr. 1, D-70569 Stuttgart, Germany, Institute of Physics, Chinese Academy of Sciences, 100190 Beijing, People's Republic of China, CNR DEMOCRITOS, Theory@Elettra Group, Istituto Officina dei Materiali IOM c/o Sincrotrone Trieste-SS14, Km 163.5, Basovizza, I-34012 Trieste, Italy, and SISSA, via Bonomea 265, I-34136 Trieste, Italy, Department of Chemistry, University of Warwick, Gibbet Hill Road, Coventry, CV4 7AL, United Kingdom, and Institut de Physique de la Matière Condensée, Ecole Polytechnique Fédérale de Lausanne (EPFL), CH-1015 Lausanne, Switzerland

Received: February 16, 2010; Revised Manuscript Received: June 3, 2010

We report on the formation of chiral domains self-assembled from terephthalic acid (TPA) and iron on a Cu(110) surface. Using scanning tunnelling microscopy, we observe that the supramolecular structures are organized on successive hierarchical levels. Chirality develops only at the latest assembly step, with the primary TPA constituents and the secondary diiron−terephthalate metal−organic complexes being mirror symmetric. The driving forces for the generation of these high-order chiral architectures are identified as competing coordination bonding within the metal−organic complexes and hydrogen bonding among them. The emergence of extended metal−organic networks is hindered by the incommensurability with the substrate.

1. Introduction

The self-assembly of organic molecules at solid surfaces results in many interesting functional nanostructures with distinctive properties.[1−4] The creation of chiral molecular structures is currently attracting increasing attention due to its potential application in nonlinear optics, surface templating, heterogeneous catalysis, and liquid-crystal technologies.[5−10] A wealth of studies demonstrates that novel low-dimensional chiral architectures can be constructed at solid surfaces from appropriate molecular building blocks.[11−23] Scanning tunnelling microscopy (STM) allows addressing molecular chirality and organization phenomena at surfaces at the level of a single molecule.[11−27] Most recent STM observations show that simple achiral molecules can form chiral arrangements on solid surfaces.[17−20,28−30] Organizational chirality is such an example and occurs when the chiral properties of supramolecular assemblies do not arise from the molecular units but from their arrangement.[6] It has recently been shown that organizational chirality can occur also in more complex two-component assemblies, in particular, in the formation of 2D coordination compounds.[18,19]

Here, we present a new manifestation of this phenomenon in adsorbed metal−organic nanostructures where chirality develops only at the last organizational level of a multistep hierarchical assembly. Our STM observations demonstrate that the coordination between the achiral terephthalic acid [TPA, HOOC−C_6H_4−COOH] and Fe atoms gives rise to likewise achiral diiron−terephathalate complexes on the Cu(110) surface. Chirality appears only at the last assembly step, which employs these metal−organic complexes as elementary components. A precise analysis of the observed structures shows that this peculiar phenomenology results from the hierarchy of the intermolecular interactions at play and from small details of the substrate geometry.

2. Methods

The experiments were performed in an ultra-high-vacuum (UHV) system providing ultimate controlled conditions for the sample preparation and characterization. The Cu(110) single crystal was cleaned by repeated cycles of Ar^+ sputtering (900 eV) and subsequent annealing at 850 K. The sample temperature was read by a K-type thermocouple directly connected to the Cu(110) crystal. Commercially available terephthalic acid (Fluka, purity = 99%) in powder form was outgassed in a Knudsen cell type evaporator and then deposited onto the Cu(110) surface held at room temperature. The temperature of the cell was kept at 445 K, as measured with a thermocouple contacted with the cell. Iron was subsequently deposited from an electron-beam evaporator. Also in this case, the surface was at room temperature. The sample was then transferred from the preparation chamber (base pressure $\sim 2 \times 10^{-10}$ mbar) to the STM chamber ($\sim 6 \times 10^{-11}$ mbar) that comprises a variable-temperature STM apparatus. STM measurements were performed at 300 K in the constant-current mode (negative U_{bias}, occupied states imaging).

The numerical simulations were based on density functional theory (DFT) with the exchange and correlation energy functional expressed in the Perdew−Burke−Ernzerhof generalized gradient approximation.[31] The Kohn−Sham equations were solved in the plane-wave pseudopotential framework, with the plane-wave basis set and the Fourier representation of the charge density being limited by kinetic cutoffs of 24 and 240 Ry, respectively. All calculations were spin-polarized. Ions were described by ultrasoft pseudopotentials.[32] Integrals in the Brillouin zone were performed on a *k*-point grid equivalent to a (12 × 12 × 12) mesh for bulk Cu, together with a Methfessel−Paxton smearing of 0.02 Ry.

The adsorption of Fe adatoms on the Cu(110) and Cu(001) surfaces was modeled by means of (5 × 3) and ($2\sqrt{2} \times 2\sqrt{2}$)

* To whom correspondence should be addressed. E-mail: g.costantini@warwick.ac.uk. Tel: +44-(0)24-765-24934. Fax: +44-(0)24-765-24112.
† Max-Planck-Institut für Festkörperforschung.
‡ Chinese Academy of Sciences.
§ Istituto Officina dei Materiali IOM c/o Sincrotrone Trieste.
∥ University of Warwick.
⊥ Ecole Polytechnique Fédérale de Lausanne (EPFL).

10.1021/jp101439z
Published on Web 07/12/2010

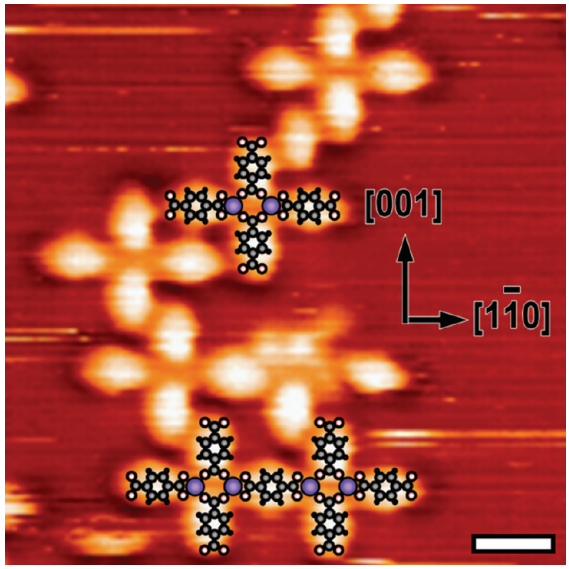

Figure 1. STM image obtained after depositing TPA and Fe on Cu(110) at 300 K. Metal−organic [$Fe_2(TPA)_4$] single and [$Fe_4(TPA)_7$] dimer complexes can be recognized together with incomplete complexes and single trapped TPA molecules. Schematic models of the complexes are superimposed on the image. Data recorded at a sample bias voltage $U_{bias} = -1.5$ V and a tunnelling current $I = 0.5$ nA. The scale bar corresponds to 1 nm.

supercells, consisting of seven and five Cu layers, respectively, and being separated by more than 10 Å of vacuum in the direction orthogonal to the surface. The atomic coordinates were relaxed according to the Hellmann−Feynman forces until the maximum force was less than 0.01 eV/Å. All calculations were performed with the Quantum-ESPRESSO computer package.[33]

3. Results and Discussion

Formation of Chiral Metal−Organic Domains. After depositing TPA molecules and iron onto Cu(110) at room temperature, two main kinds of structures were observed both in the form of flowerlike complexes, as shown in Figure 1. The first one includes four bright elliptic protrusions, two of them being aligned along the [1$\bar{1}$0] direction of the Cu(110) surface, the other two along [001]. We dub this assembly, similar to a four-petal flower, as a *single complex*. The other kind of observed structure is composed of seven bright protrusions and is termed a *dimer complex*. The individual protrusions are readily assigned to single flat-lying molecules because their size and shape agree well with those of the TPA molecule (length of ∼7.0 Å in the relaxed configuration). A further proof is given by the similarity of the present protrusions with those measured for TPA−Fe networks assembled on different substrates.[34,35] All these systems present the same structural motif, whose cohesion is determined by the presence of a dimer of Fe atoms forming two chelating and two bridging metal−organic bonds with the carboxylate groups of the TPA molecules.

This comparison allow us to conclude that, although not directly visible by STM, a pair of iron atoms is located at the flower center also in the present case, as shown in the superimposed models in Figure 1. In fact, the same binding motif has been observed also for linear benzene-dicarboxylic acids on Cu(001),[34−37] Au(111),[38,39] and Ag(111).[40] In particular, on Cu(001), this motif gives rise to extended two-dimensional (2D) porous networks.[34−37]

TPA molecules bind to the adjacent Fe atoms through their deprotonated carboxylate terminals [COO^-]. The deprotonation

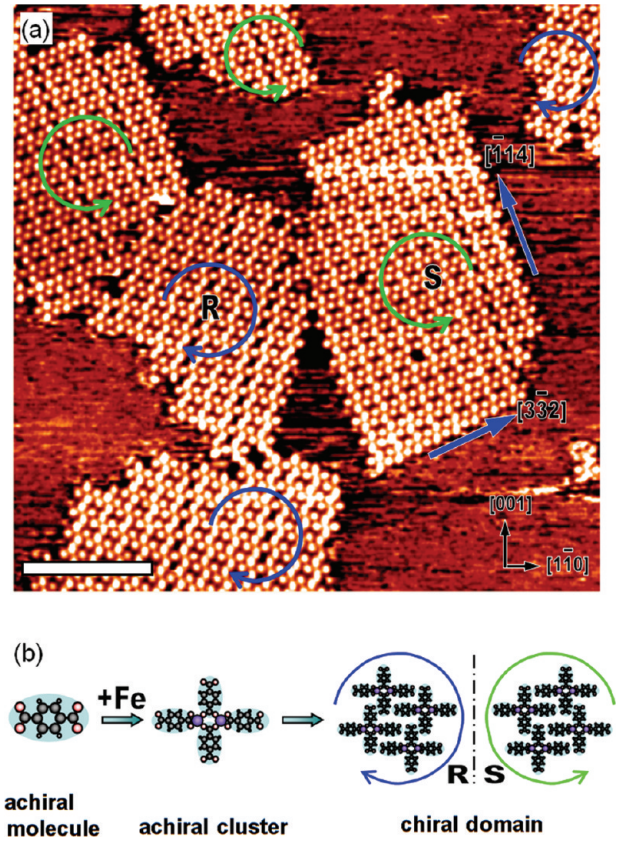

Figure 2. (a) STM image of well-ordered chiral domains after sample annealing at 430 K. $U_{bias} = -2.0$ V, $I = 0.5$ nA. The scale bar corresponds to 10 nm. R- and S-chiral domains are denoted by clockwise and anticlockwise arrows, respectively. The directions of the main domain edges are explicitly indicated. (b) Schematics of the hierarchical assembly: primary achiral TPA molecule, secondary achiral Fe−TPA complex, and tertiary chiral domains.

of carboxylic groups at Cu surfaces has been confirmed for several benzoic acid species through a variety of experimental and theoretical methods, including photoemission spectroscopy, reflection adsorption infrared spectroscopy, and DFT calculations.[35,41−45] The loss of hydrogen atoms appears to be an activated process, with a characteristic temperature depending on the specific orientation of the Cu substrate. In particular, room-temperature deprotonation of carboxylic moieties has been reported for Cu(110).[41−43] The underlying metal substrate partially screens the negative charges of the carboxylate moieties[46] that coordinatively bind to the metal adatoms.[44]

Independent of the coverage and of the Fe/TPA ratio, we found that a distribution of Fe−TPA flowerlike complexes is formed at room temperature on Cu(110) with some local order but without any long-range periodicity. With the aim of reproducing the extended networks observed on Cu(001), we annealed the sample to 430 K for several minutes to enhance the surface mobility. The heating treatment effectively drives the development of well-ordered 2D supramolecular domains, as illustrated in the representative STM image of Figure 2a. However, these Fe−TPA assemblies do not form an extended and continuous porous network. On the contrary, it is easy to recognize that these regular structures result from the direct juxtaposition of single and dimer complexes. The short distance between the molecules in neighboring complexes suggests the existence of intermolecular ionic hydrogen bonding;[46] see Figure 3. One oxygen atom of a TPA molecule couples with the H atoms of the phenyl ring of the adjacent TPA, as illustrated by

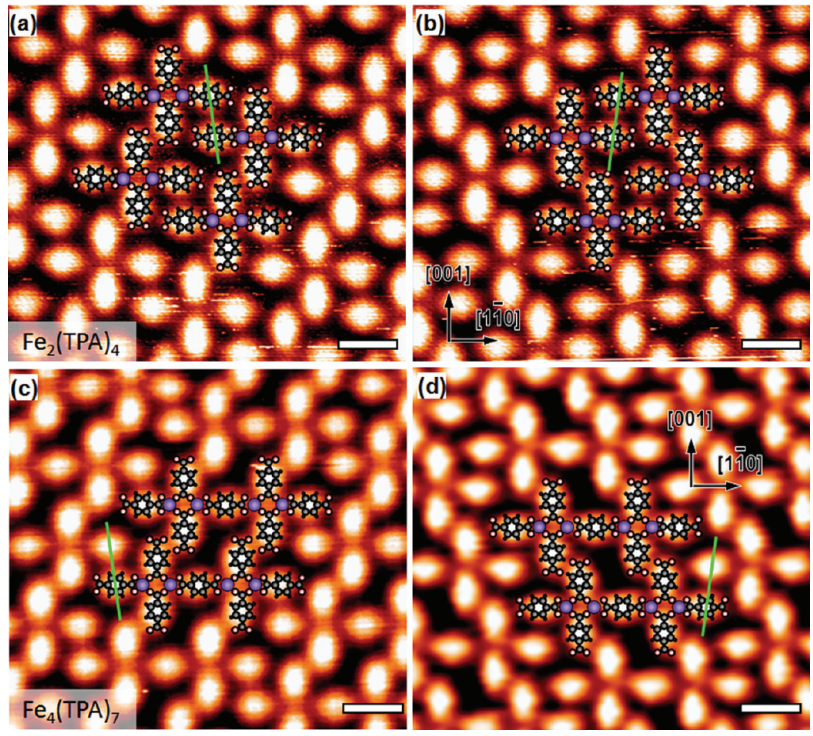

Figure 3. High-resolution STM images of the chiral Fe−TPA domains on Cu(110). (a) R domain and (b) S domain composed of $[Fe_2(TPA)_4]$ single complexes. (c) R domain and (d) S domain composed of $[Fe_4(TPA)_7]$ dimer complexes. $U_{bias} = -1.8$ V, $I = 0.5$ nA, scale bar = 1 nm. The green lines show the directions joining the centers of two equivalent TPA molecules in neighboring complexes. Notably, these form angles of ca. ± 7° with the [001] direction.

the dashed line in Figure 4a. The O···H−C length is estimated to be 2.35 Å, which is in the range of ideal hydrogen-bond lengths.[47] These double hydrogen bonds exist between two [001]-oriented TPA molecules of neighboring complexes, although other, weaker H bonds might be present as well. In fact, the supramolecular islands show straight edges oriented along [$\bar{1}$14] but also along [3$\bar{3}$2]; see Figure 2a. The former edge is stabilized by the ionic hydrogen bonds described above, but the latter indicates the existence of further attractive interactions between the metal−organic complexes. The difference in strength between these two types of bonds is reflected in the unequal extension of the two edges.

The complexes organize in separate mirror-symmetric R and S supramolecular islands identified by the clockwise and anticlockwise round arrows in Figure 2a, respectively. Figure 3 shows close-up STM images of such islands and demonstrates that both $[Fe_2(TPA)_4]$ single complexes (Figure 3a,b) and $[Fe_4(TPA)_7]$ dimer complexes (Figure 3c,d) can act as building blocks for the R and S domains. The chirality of these domains stems from the organization of the Fe−TPA complexes. In fact, given that an isolated complex represents the nucleus for an extended island, there exist four equally probable H-binding sites for a second complex. Two of them, in the lower left and the upper right corners, will start an R-oriented domain (Figure 3a,c), whereas the remaining two, in the lower right and the upper left corners, will generate an S domain (Figure 3b,d). Once established, a domain will grow by guarding its chirality because this maximizes the 2D packing of the complexes and, therefore, minimizes the energy of the system. As a consequence, all supramolecular islands show either R or S chirality and form dislocation lines when meeting, as can be seen in Figure 2a.

The manifestation of chirality in the TPA/Cu(110) system occurs only at the latest stage of supramolecular organization. As a matter of fact, as denoted in the schematics in Figure 2b, the primary organizational level is characterized by achiral building blocks, the TPA molecules themselves. The units of the secondary level, that is, the Fe−TPA single and dimer complexes, are still achiral, and it is only at the tertiary level that chirality sets in. This is different to what is observed in other systems,[48] even in similar 2D metal−organic ones.[19] To our knowledge, this kind of higher-order organizational chirality has hitherto not been reported in any surface-supported self-assembled supramolecular system.

Absence of Extended Metal−Organic Networks. Even after the annealing treatment, the great majority of the metal−organic complexes observed by STM is composed of $[Fe_2(TPA)_4]$ single complexes (representing typically more than 60% of the population, the exact value depending on the deposited Fe/TPA ratio) or $[Fe_4(TPA)_7]$ dimer complexes. Trimer complexes were also occasionally observed (<5%), but longer [1$\bar{1}$0]-oriented $[Fe_{2n}(TPA)_{3n+1}]$ chains with $n > 3$ were never seen. Moreover, the formation of extended Fe−TPA metal−organic structures along the [001] direction was never observed. To check whether this depends on the Fe/TPA ratio, we performed a series of experiments under the same deposition and annealing conditions, with the relative amount of Fe and TPA as the only varying parameter. The results clearly demonstrate that the preference for single over dimer or trimer complexes as well as the absence of extended 2D porous networks is not caused by a lack of iron coordination centers. Figure 5 shows a typical STM image for the high Fe/TPA regime. Agglomerates formed by excess iron can be recognized on the surface without any change in the local Fe/TPA stoichiometry. Because the annealing step excludes any significant role of kinetic limitations, energetic reasons must regulate the preference of TPA molecules and Fe atoms to form chiral arrays of flowerlike complexes instead of extended metal−organic networks on Cu(110).

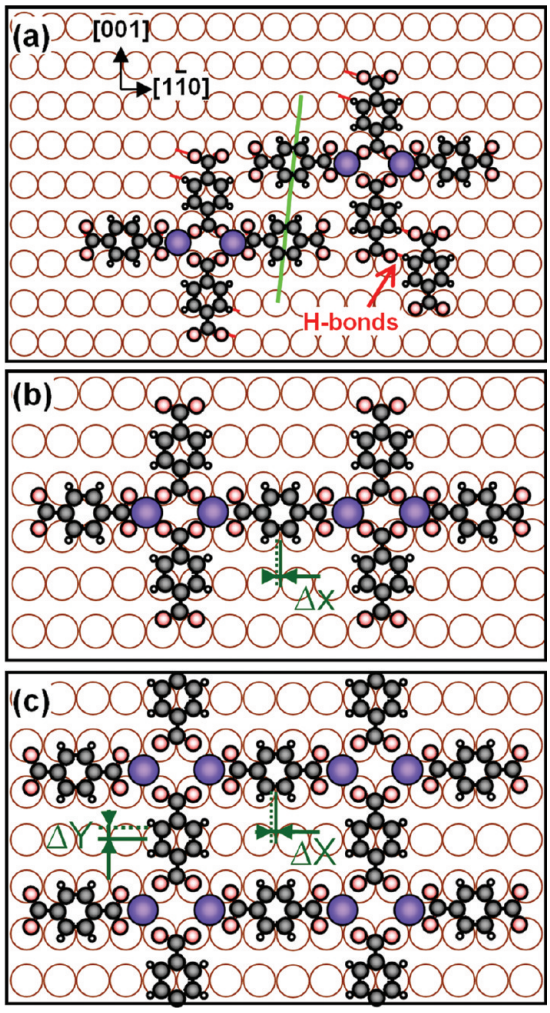

Figure 4. Atomistic models of (a) $[Fe_2(TPA)_4]$ single complexes, (b) $[Fe_4(TPA)_7]$ dimer complexes, and (c) an ideal extended diiron−TPA network on Cu(110). Red lines in (a) represent the intermolecular double H bonds, whereas green lines join the centers of equivalent TPA molecules in neighboring complexes. (c) ΔX and ΔY denote the ideal [1$\bar{1}$0] and [001] shifts in the position of the TPA molecules with respect to the single complex configuration shown in (a).

To further rationalize these observations, it is helpful to accurately examine the structure of the supramolecular arrangements. In analogy to what is established for similar systems,[35] the position of the Fe atoms can safely be identified close to the hollow sites of the substrate atomic lattice. This assignment also defines the position of the carboxylate O atoms relative to the substrate and, as a consequence, the position of the whole molecule. TPA molecules show two kinds of absorption configurations on Cu(110): with the phenyl ring close to the substrate short-bridge sites for the [001]-oriented TPAs or near the 4-fold hollow site for the [1$\bar{1}$0]-oriented TPAs, as depicted in Figure 4a. High-resolution STM images reveal that, in single complexes, the distances between the centers of [1$\bar{1}$0]- and [001]-oriented TPA molecules are 14.6 ± 0.2 and 9.0 ± 0.3 Å, respectively. In dimer complexes, the central TPA molecule is symmetrically attracted by two diiron pairs and its distances from the lateral molecules along [1$\bar{1}$0] becomes 14.9 ± 0.3 Å. On the other hand, the distance between the [001]-oriented TPAs remains the same. These values are equivalent to ∼5.7 to 5.8 times the substrate periodicity along [1$\bar{1}$0] (2.556 Å) and ∼2.5 times along [001] (3.615 Å). Thus, the Cu(110) lattice would be incommensurate with an extended 2D metal−organic network of diiron centers and TPA molecules with a unit cell based on the structural parameters of single or double complexes. This is, for example, reflected in the fact that the line joining the centers of two equivalent TPA molecules in neighboring single and dimer complexes (green lines in Figure 3) is not oriented along the substrate [001] direction but forms an angle of ca. ± 7° with respect to this direction.

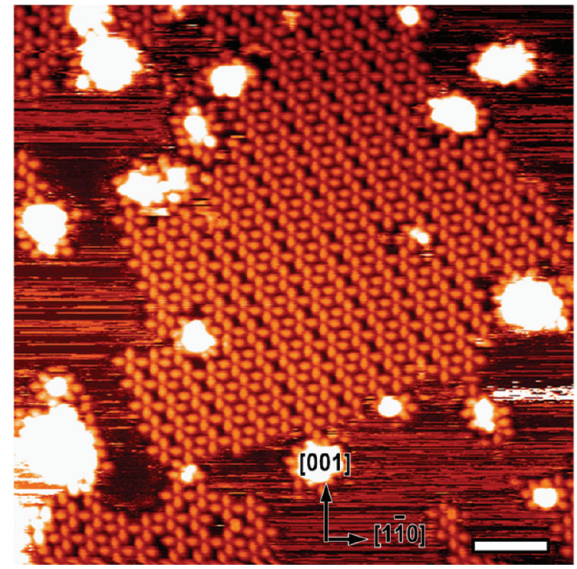

Figure 5. STM image representative of the high Fe/TPA ratio regime after annealing at 430 K. $U_{bias} = -2.5$ V, $I = 0.6$ nA, scale bar is 5 nm. Excess iron organizes into clusters (bright spots) without any significant change in the local Fe−TPA stoichiometry.

Our measurements clearly indicate that the configuration for which the molecules are closest to the diiron centers (single complex) is the most frequent and, as a consequence, the lowest energy one. This implies that the driving force for the observed assembly is the establishment of Fe−O distances allowing the formation of strong metal−organic bonds. In dimer complexes, the intermolecular distance along [1$\bar{1}$0] is about 0.3 Å larger than that in single complexes. This clearly results in a bigger Fe−O separation, which stretches the metal−organic bond and makes it less favorable but still possible. For an ideal infinite [1$\bar{1}$0]-aligned Fe−TPA chain, each in-plane Fe−O distance would be about 0.37 Å longer than that for single complexes. The absence of $[Fe_{2n}(TPA)_{3n+1}]$ complexes with $n > 3$ indicates that this increase would be excessive for the formation of a strong bond. The situation would be even more extreme along [100], with an in-plane Fe−O distance about 0.9 Å larger than that for single complexes. Thus, most probably, the reason why extended networks are never observed on Cu(110) is that they would require excessively big Fe−O distances. On the other hand, single and dimer complexes can interact among each other by means of much more flexible hydrogen bonds, resulting in the chiral arrangements described above.

A final important issue to be discussed is the difference between the nanostructures formed on Cu(001) and Cu(110). We note that, in the case of the Cu(001) surface, very regular metal−organic networks are developed, being formed by the same $[Fe_2(TPA)_4]$ elemental unit discussed above.[34,35,44] In this case, the interface with the substrate is coherent along both [110] and [1$\bar{1}$0], thus determining a natural periodicity of the metal−organic network of 10.2 and 15.3 Å, respectively.

Because the atomic lattice periodicity along [110] is a factor of $\sqrt{2}$ larger on Cu(110) than on Cu(001), it not surprising that a regular [110]-oriented structure is not developed on the former surface. However, the periodicity of the two substrates is

identical along [1$\bar{1}$0] so that the development of longer [1$\bar{1}$0] diiron−TPA chains could be expected also on Cu(110). Their absence rules out that sole in-plane structural properties govern the formation of extended Fe−TPA structures. Most probably, the reason why only single and dimer complexes are observed on Cu(110) lies in the openness of its lattice and thus in its geometrical characteristics perpendicular to the surface.

Our DFT calculations show that a single Fe atom positioned in the 4-fold hollow site is located 0.3 Å lower on Cu(110) than on Cu(001). In agreement with previous DFT calculations,[35] we find that the development of Fe−O metal−organic bonds displaces the Fe adatoms from their isolated equilibrium hollow sites. In the surface plane, this displacement is by 0.3 Å, which is small (0.13%) on the scale of the lattice vectors; thus, the Fe adatoms can still be considered to be overall above the hollow site. This effect is more significant in the direction perpendicular to the surface where upward lifts of 0.6 Å have been reported for the Fe−TPA/Cu(001) system[35] and of 0.3 Å for the Fe−TMA/Cu(110) system. The absolute positions of the oxygen-coordinated Fe atoms might thus be slightly higher than the DFT values obtained for isolated Fe adatoms. However, the relative difference between Cu(110) and Cu(001) should remain qualitatively the same.

Assuming that the average height of TPA is similar on both substrates, this implies that, on Cu(110), the molecules must move closer to the hollow site occupied by the Fe atom in order to attain the same Fe−O distance and thus to form an effective metal−organic bond. This is straightforward for single clusters and is in accordance with the smaller in-plane TPA−TPA distance obtained from the STM data. In double clusters, the external TPA molecules can move closer to the neighboring Fe hollow sites but the central one must clearly occupy a symmetric position (Figure 4b). As a consequence, two out of the four metal−organic bonds formed by [1$\bar{1}$0]-oriented TPA molecules will be strained and thus energetically less favorable. Nevertheless, the overall energy balance must still be acceptable because double clusters are experimentally observed. Most probably, this is not the case for extended diiron−TPA assemblies that were never observed on Cu(110). This could explain why the same in-plane lattice periodicity allows the formation of extended metal−organic networks in the case of a (001) but not of a (110) surface.

It should be further noted that the difference in the height of the Fe centers might also be the reason for the difference in the STM images, where coordinated Fe atoms appear as distinct protrusions on Cu(001)[34,35,44] but are not visible on Cu(110). The same effect could be responsible also for the different appearance of the metal center in mononuclear Fe−trimesate complexes on Cu(001)[19] and Cu(110).[49]

4. Conclusion

In summary, we have presented a detailed analysis of the chiral nanostructures formed by self-assembly of Fe and TPA on the Cu(110) surface. High-resolution STM images reveal different types of building blocks organized in subsequent hierarchical levels: TPA molecules, metal−organic [$Fe_2(TPA)_4$] and [$Fe_4(TPA)_7$] complexes, and their H-bond-mediated assemblies. Interestingly, chirality emerges only at the ultimate level of organization. In fact, neither the primary molecular components nor the secondary metal−organic complexes are chiral. Only the tertiary assembly stage displays the absence of mirror symmetry and the development of organizational chirality. By precisely assessing the structural characteristics of the Fe−TPA architectures, we have expounded the driving force for the formation of the chiral motifs. These result from the interplay between the openness and the anisotropy of the Cu(110) surface lattice, the coordination interaction between the molecular carboxylate moieties and the Fe centers, and the intermolecular hydrogen attraction. Metal−organic bonds form in the first instance because of their higher binding energy. However, they develop only locally because their extension in the form of a periodic network is frustrated by the incommensurability with the underlying substrate. In particular, we have shown that, although the local structure of the diiron−TPA synthons is analogous to what is observed for other substrates, the absence of extended metal−organic networks is due to the detailed 3D absorption potential of the Cu(110) surface. Finally, only weaker and more flexible H bonds are established between the metal−organic units.

Our results clearly demonstrate the importance of the substrate for the formation of supported molecular nanoarchitectures. Even small differences and specific details of the surface structure can determine not only the geometry but also the chirality of supramolecular assemblies. These effects must, therefore, carefully be taken into account when considering the formation of chiral surfaces and phenomena, such as chiral templation.

Acknowledgment. Helpful discussions with Nian Lin, Thomas Classen, and Magalí Lingenfelder are gratefully acknowledged. The Rechenzentrum Garching (RZG) of the Max-Planck Society is kindly acknowledged for providing computational resources.

References and Notes

(1) Lehn, J. M. *Proc. Natl. Acad. Sci. U.S.A.* **2002**, *99*, 4763.
(2) Forrest, S. R. *Chem. Rev.* **1997**, *97*, 1793.
(3) Barth, J. V.; Costantini, G.; Kern, K. *Nature* **2005**, *437*, 671.
(4) Barth, J. V. *Annu. Rev. Phys. Chem.* **2007**, *58*, 375.
(5) Yaghi, O. M.; O'Keeffe, M.; Ockwig, N. W.; Chae, H. K.; Eddaoudi, M.; Kim, J. *Nature* **2003**, *423*, 705.
(6) Barlow, S. M.; Raval, R. *Surf. Sci. Rep.* **2003**, *50*, 201.
(7) Yoon, T. P.; Jacobsen, E. N. *Science* **2003**, *299*, 1691.
(8) Lemieux, R. P. *Acc. Chem. Res.* **2001**, *34*, 845.
(9) Barbera, J.; Giorgini, L.; Paris, F.; Salatelli, E.; Tejedor, R. M.; Angiolini, L. *Chem.—Eur. J.* **2008**, *14*, 11209.
(10) Lin, S. C.; Lin, T. F.; Ho, R. M.; Chang, C. Y.; Hsu, C. S. *Adv. Funct. Mater.* **2008**, *18*, 3386.
(11) Hermse, C. G. M.; vanBavel, A. P.; Jansen, A. P. J.; Barbosa, L. A. M. M.; Sautet, P.; vanSanten, R. A. *J. Phys. Chem. B* **2004**, *108*, 11035.
(12) Fasel, R.; Parschau, M.; Ernst, K. H. *Angew. Chem., Int. Ed.* **2003**, *42*, 5178.
(13) Chen, Q.; Richardson, N. V. *Nat. Mater.* **2003**, *2*, 324.
(14) De Feyter, S.; Gesquière, A.; Wurst, K.; Amabilino, D. B.; Veciana, J.; Schryver, F. C. D. *Angew. Chem., Int. Ed.* **2001**, *40*, 3217.
(15) Lorenzo, M. O.; Baddeley, C. J.; Muryn, C.; Raval, R. *Nature* **2000**, *404*, 376.
(16) Jones, T. E.; Baddeley, C. J. *Surf. Sci.* **2002**, *513*, 453.
(17) Weckesser, J.; De Vita, A.; Barth, J. V.; Cai, C.; Kern, K. *Phys. Rev. Lett.* **2001**, *87*, 096101.
(18) Messina, P.; Dmitriev, A.; Lin, N.; Spillmann, H.; Abel, M.; Barth, J. V.; Kern, K. *J. Am. Chem. Soc.* **2002**, *124*, 14000.
(19) Spillmann, H.; Dmitriev, A.; Lin, N.; Messina, P.; Barth, J. V.; Kern, K. *J. Am. Chem. Soc.* **2003**, *125*, 10725.
(20) Katano, S.; Kim, Y.; Matsubara, H.; Kitagawa, T.; Kawai, M. *J. Am. Chem. Soc.* **2007**, *129*, 2511.
(21) Wang, Y.; Lingenfelder, M.; Classen, T.; Costantini, G.; Kern, K. *J. Am. Chem. Soc.* **2007**, *129*, 15742.
(22) Huang, T.; Hu, Z. P.; Zhao, A. D.; Wang, H. Q.; Wang, B.; Yang, J. L.; Hou, J. G. *J. Am. Chem. Soc.* **2007**, *129*, 3857.
(23) Kuck, S.; Hoffmann, G.; Broring, M.; Fechtel, M.; Funk, M.; Wiesendanger, R. *J. Am. Chem. Soc.* **2008**, *130*, 14072.
(24) Weigelt, S.; Busse, C.; Petersen, L.; Rauls, E.; Hammer, B.; Gothelf, K. V.; Besenbacher, F.; Linderoth, T. R. *Nat. Mater.* **2006**, *5*, 112.
(25) Böhringer, M.; Morgenstern, K.; Schneider, W. D.; Berndt, R. *Angew. Chem., Int. Ed.* **1999**, *38*, 821.

(26) Lopinski, G. P.; Moffatt, D. J.; Wayner, D. D.; Wolkow, R. A. *Nature* **1998**, *392*, 909.
(27) Kühnle, A.; Linderoth, T. R.; Hammer, B.; Besenbacher, F. *Nature* **2002**, *415*, 891.
(28) Xiao, W.; Feng, X.; Ruffieux, P.; Groning, O.; Mullen, K.; Fasel, R. *J. Am. Chem. Soc.* **2008**, *130*, 8910.
(29) Ernst, K.-H. *Curr. Opin. Colloid Interface Sci.* **2008**, *13*, 54.
(30) Schlickum, U.; Decker, R.; Klappenberger, F.; Zoppellaro, G.; Klyatskaya, S.; Auwarter, W.; Neppl, S.; Kern, K.; Brune, H.; Ruben, M.; Barth, J. V. *J. Am. Chem. Soc.* **2008**, *130*, 11778.
(31) Perdew, J. P.; Burke, K.; Ernzerhof, M. *Phys. Rev. Lett.* **1996**, *77*, 3865.
(32) Vanderbilt, D. *Phys. Rev. B* **1990**, *41*, 7892.
(33) Giannozzi, P.; Baroni, S.; Bonini, N.; Calandra, M.; Car, R.; Cavazzoni, C.; Ceresoli, D.; Chiarotti, G.; Cococcioni, M.; Dabo, I.; Dal Corso, A.; de Gironcoli, S.; Fabris, S.; Fratesi, G.; Gebauer, R.; Gerstmann, U.; Gougoussis, C.; Kokalj, A.; Lazzeri, M.; Martin-Samos, L.; Marzari, N.; Mauri, F.; Mazzarello, R.; Paolini, S.; Scandolo, S.; Sclauzero, G.; Seitsonen, A.; Smogunov, A.; Umari, P.; Wentzcovitch, R. *J. Phys.: Condens. Matter* **2009**, *21*, 395502.
(34) Lingenfelder, M. A.; Spillmann, H.; Dmitriev, A.; Stepanow, S.; Lin, N.; Barth, J. V.; Kern, K. *Chem.—Eur. J.* **2004**, *10*, 1913.
(35) Seitsonen, A. P.; Lingenfelder, M.; Spillmann, H.; Dmitriev, A.; Stepanow, S.; Lin, N.; Kern, K.; Barth, J. V. *J. Am. Chem. Soc.* **2006**, *128*, 5634.
(36) Dmitriev, A.; Spillmann, H.; Lin, N.; Barth, J. V.; Kern, K. *Angew. Chem., Int. Ed.* **2003**, *41*, 2670.
(37) Stepanow, S.; Lingenfelder, M.; Dmitriev, A.; Spillmann, H.; Delvigne, E.; Lin, N.; Deng, X.; Cai, C.; Barth, J. V.; Kern, K. *Nat. Mater.* **2004**, *3*, 229.
(38) Clair, S.; Pons, S.; Brune, H.; Kern, K.; Barth, J. V. *Angew. Chem., Int. Ed.* **2005**, *44*, 7294.
(39) Clair, S.; Pons, S.; Fabris, S.; Baroni, S.; Brune, H.; Kern, K.; Barth, J. V. *J. Phys. Chem. B* **2006**, *110*, 5627.
(40) Suzuki, T.; Lutz, T.; Payer, D.; Lin, N.; Tait, S. L.; Costantini, G.; Kern, K. *Phys. Chem. Chem. Phys.* **2009**, *11*, 6498.
(41) Perry, C. C.; Haq, S.; Frederick, B. G.; Richardson, N. V. *Surf. Sci.* **1998**, *409*, 512.
(42) Martin, D. S.; Cole, R. J.; Haq, S. *Phys. Rev. B* **2002**, *66*, 155427.
(43) Classen, T.; Fratesi, G.; Costantini, G.; Fabris, S.; Stadler, F. L.; Kim, C.; de Gironcoli, S.; Baroni, S.; Kern, K. *Angew. Chem., Int. Ed.* **2005**, *44*, 6142.
(44) Tait, S. L.; Wang, Y.; Costantini, G.; Lin, N.; Baraldi, A.; Esch, F.; Petaccia, L.; Lizzit, S.; Kern, K. *J. Am. Chem. Soc.* **2008**, *130*, 2108.
(45) Cortes, R.; Mascaraque, A.; Schmidt-Weber, P.; Dil, H.; Kampen, T. U.; Horn, K. *Nano Lett.* **2008**, *8*, 4162.
(46) Payer, D.; Comisso, A.; Dmitriev, A.; Strunskus, T.; Lin, N.; Woll, C.; DeVita, A.; Barth, J. V.; Kern, K. *Chem.—Eur. J.* **2007**, *13*, 3900.
(47) Barbosa, L. A. M. M.; Sautet, P. *J. Am. Chem. Soc.* **2001**, *123*, 6639.
(48) Humblot, V.; Barlow, S. M.; Raval, R. *Prog. Surf. Sci.* **2004**, *76*, 1.
(49) Classen, T.; Lingenfelder, M.; Wang, Y.; Chopra, R.; Virojanadara, C.; Starke, U.; Costantini, G.; Fratesi, G.; Fabris, S.; de Gironcoli, S.; Baroni, S.; Haq, S.; Raval, R.; Kern, K. *J. Phys. Chem. A* **2007**, *111*, 12589.

JP101439Z